

# Spin-orbit coupling induced Dirac monopoles with polar-core vortex in spinor Bose-Einstein condensates

Ji Li, Yan-Mei Yu, and Wu-Ming Liu\*

<sup>1</sup>*Beijing National Laboratory for Condensed Matter Physics, Institute of Physics, Chinese Academy of Sciences, Beijing 100190, China*

\*e-mail: [wliu@iphy.ac.cn](mailto:wliu@iphy.ac.cn)

Magnetic monopoles describe isolated north or south magnetic poles. The practical detection of the free magnetic monopoles, due to their extremely heavy masses, remains challenging so far. However, Bose-Einstein condensates offer an ideal observable platform for probing monopoles. In particular, the recent realization of spin-orbit (SO) coupling, owing to its high controllability and tunability, provides an unprecedented opportunity to explore exotic structures and phase transitions of monopoles unrealizable elsewhere. Here we report Dirac monopoles attached to the polar-core vortex induced by SO coupling in ferromagnetic Bose-Einstein condensates, which can be readily observed via time of flight measurements in experiment. The results show that, a cyclic phase transition from Dirac monopoles with polar-core vortex to that with Mermin-Ho vortex, is induced by SO coupling. Our studies may open a new direction to realize exotic topological defects and phase transitions in quantum systems.

Dirac monopoles, that are, the point sources of magnetic fields, are attached to at least one terminating nodal line, such the semi-infinite nodal line is called Dirac string in physics. Dirac

predicted the existence of the monopoles in order to explain the quantization of electric charge for the first time<sup>1</sup>. From then on, the monopoles have been attracted more and more attention, and have been studied in a wide area of research in solid state physics<sup>2-7</sup>, the quantum field<sup>8,9</sup>, and other systems<sup>10-13</sup>. In addition, people have attempted to seek the free magnetic monopoles in cosmic rays and particle accelerators, but there has not yet been firm evidence for their existence due to their extremely heavy masses. Fortunately, Bose-Einstein condensates offer an ideal platform for probing the details of monopoles. More recently, the realization of multi-component Bose-Einstein condensates in optical traps has made it possible to create a variety of topologically nontrivial structures, such as vortices<sup>14</sup>, skyrmions<sup>15,16</sup>, and monopoles<sup>17,18</sup>. By now, two examples of the monopoles, called wave-function monopoles<sup>19</sup> and spin monopoles<sup>20</sup>, which have been studied in two-component Bose-Einstein condensates. Ground-states and dynamics of monopoles have also been discussed in ferromagnetic and antiferromagnetic systems with gradient magnetic field<sup>21-23</sup>. Non-Abelian magnetic monopole subjected to an effective magnetic field is also observed<sup>24,25</sup>, in addition, several types of monopoles in other systems have been worked out theoretically<sup>26-28</sup>. On the other hand, Dirac monopoles in Bose-Einstein condensates with a synthetic magnetic field have been observed by the time-of-flight absorption imaging technique<sup>8</sup>, furthermore, the isolated monopoles in quantum systems have been realized through experiment<sup>9</sup>. In the previous works, a majority of studies the corresponding monopoles have been made in Bose-Einstein condensates without any gauge potential, but there has not yet been reported the monopoles with spin-orbit coupling. Indeed, the realization of multi-dimensional spin-orbit coupling for the system with high spin, due to couple more atomic states, remains challenging. The investigations of monopoles

subjected to spin-orbit interaction are still lacking so far.

Spin-orbit (SO) coupling, describes interaction between the spin of a quantum particle and its momentum, is a ubiquitous quantum phenomenon in physical systems. Recent predictions of topological states in condensed matter relied on SO coupling<sup>29,30</sup>. In solid-state materials, SO coupling originates from electrons moving in the crystal field, in which is only adjusted slightly in the experiment, owing to its strength have to be determined by the specific material parameters. In contrast, for Bose-Einstein condensates, in which SO coupling, generated with the help of optical fields or a sequence of pulsed homogeneous magnetic fields, is controllable and tunable at will. Very recently, the synthetic SO coupling in Bose-Einstein condensates has been first realized by the coupling of atoms to laser beams<sup>31</sup>, this opens up a new research direction in cold atom physics. During the last few years, a number of SO coupling schemes in ultracold atoms have been reported in experiments and theories<sup>32-41</sup>. It provides opportunities to search for novel quantum states and other rich topological structures in Bose-Einstein condensates, such as the plane wave<sup>42</sup>, density stripe<sup>42</sup>, half-skyrmion<sup>43,44</sup>, vortex lattice<sup>45</sup>, fractional vortex<sup>46</sup>, skyrmion lattice<sup>47</sup>, quantum quasicrystals<sup>48</sup>, and supersolid state<sup>49,50</sup>. This raises a question what is the physics of monopoles with SO coupling. In particular, in a recent the monopole study, it is found that the pseudospin texture with a topological charge cancels the monopole charge in the effective non-Abelian magnetic field<sup>24</sup>, this inspires that the monopole could displays more rich properties if subjected to the non-Abelian gauge field like SO coupling. As we known, the synthetic SO coupling in Bose-Einstein condensates, due to their cleanliness and high tunability, provides an unprecedented opportunity to explore exotic structures and phase transitions of monopoles unrealizable elsewhere, these mo-

tivate us to investigate the monopole with respect to SO coupling.

In this work, we demonstrate Dirac monopoles attached to polar-core vortex induced by weak SO coupling in ferromagnetic Bose-Einstein condensates, where the condensates are subjected to three-dimensional gradient magnetic field, generated by means of a pair of Helmholtz coils, and two dimensional Rashba-type SO coupling induced by magnetic pulses. Our results show that, a cyclic phase transition from Dirac monopoles with polar-core vortex to that with Mermin-Ho vortex, is induced by SO coupling. For the strong SO coupling case, we observe the square lattice phase, particularly, the square lattice is extraordinary distinct in the central zone of Bose-Einstein condensates, meanwhile, the density distribution of its longitudinal direction similar to stripe structures. Furthermore, when SO coupling is anisotropic, an interesting result is observed that the monopoles disappear, whereas the stripe phase similar to that predicted for isotropy SO coupling condensates can emerge. Finally, we obtain entire phase diagrams from the nontrivial interplay between SO coupling, spin-dependent interactions and spin-independent interactions. The presence of the monopoles can be proved through directly imaging the vortex lines in experiment<sup>8</sup>, therefore, the readily detection of the monopoles accompanied with vortex structures can be realized via time of flight absorption imaging technique in a real experiment.

## Results

**Spin-orbit coupling induced by magnetic pulses.** We consider spin-1 Bose-Einstein condensates of alkali <sup>87</sup>Rb atoms. The scheme for creating two-dimensional Rashba-type SO coupling is

illustrated in Fig. 1a, we take  $^{87}\text{Rb}$  Bose-Einstein condensates consist of  $0.6(1.8) \times 10^5$  atoms, the cloud of atoms is trapped  $50\mu\text{m}$  above the surface of an atom chip. Here, SO coupling is produced via magnetic pulses<sup>39</sup>. In the beginning, a strong time-independent bias magnetic field with respect to out of plane is applied<sup>39</sup>, and it leads to splitting among magnetic sublevels. In order to achieve magnetic pulses, we use simultaneously two rf magnetic fields in the x-y plane, such two rf magnetic fields are produced by means of two pairs of microwires embedded in the chip. The process of creating SO coupling can be divided into the two stages. The first stage ( $0 \leq t < \tau$ ), the rf magnetic field  $\mathbf{B}_x$  with frequency  $\omega$  leads to an effective coupling vector along x direction, and a spin-dependent phase gradient along y direction, here, SO coupling can be written as  $-i\hbar\kappa_x F_x \partial_x$ . The second stage ( $\tau \leq t < 2\tau$ ), the rf magnetic field  $\mathbf{B}_y$  with frequency  $\omega$  arrives at an effective coupling vector along y direction, and a spin-dependent phase gradient along x direction. In this case, SO coupling can be written as  $-i\hbar\kappa_y F_y \partial_y$ . When these two stages together, it can provide a 2D SO coupling  $\mathcal{V}_{so} = -i\hbar(\kappa_x F_x \partial_x + \kappa_y F_y \partial_y)$  in the first-order approximation<sup>39</sup>. The strength of SO coupling  $\kappa_x$  and  $\kappa_y$  depend on the strength of the magnetic field gradient. In fact, the quadratic Zeeman term in Hamiltonian, it hardly to affect the ground state phases, so we only consider the first-order approximation. Indeed, for  $\kappa_x = \kappa_y$ , the isotropic Rashba-type SO coupling is obtained.

On the other hand, experimentally, the synthetic magnetic field is realized by two quadrupole fields, such quadrupole fields have been proven to generate a knot structure in antiferromagnetic Bose-Einstein condensates<sup>51</sup>. The fields are produced by a crossing pair of Helmholtz coils [illustrated Fig. 1b], the intensity of the electric current in the coils is equal, but the direction of current is opposite. There exists a point M, where the external magnetic field vanished, meanwhile, when

the distance from center is increased, magnetic field intensity is enlarged linearly, such the point M is also the center of a monopole defect. Monopole-free field distribution looks like as the radially outward hedgehog form [see Fig. 1d]. Due to Rashba SO coupling, the spin degeneracy of three component bosons is lifted, the free particle energy spectrum splits into three energy branches with different helicity [see Fig. 1c]. Furthermore, we can see a black circular ring from the minimum energy spectrum, such a black circular ring represents a Rashba ring.

**Dirac monopoles.** We consider Dirac monopoles that arises in the context of a three-dimensional ferromagnetic spin-1 Bose-Einstein condensates with a pure Rashba type SO coupling<sup>39</sup>, in addition, the modifying external magnetic fields is used in this system<sup>8</sup>. In the mean-field approximation, the Hamiltonian for the spin-1 Bose-Einstein condensates with an optical trap is

$$H = \int d^3\mathbf{r} \left\{ \Psi^\dagger \left( -\frac{\hbar^2 \nabla^2}{2m} + V_{opt}(\mathbf{r}) + \mathcal{V}_{so} + g_F \mu_B \mathbf{B}(\mathbf{r}) \cdot \mathcal{F} \right) \Psi + \left( \frac{c_0}{2} n^2 + \frac{c_2}{2} [(n_1 - n_{-1})^2 + 2|\Psi_1^* \Psi_0 + \Psi_0^* \Psi_{-1}|^2] \right) \right\}, \quad (1)$$

here, the condensate order parameter  $\Psi = [\Psi_1(\mathbf{r}), \Psi_0(\mathbf{r}), \Psi_{-1}(\mathbf{r})]^T$ , and the complex-valued order parameter is normalized to satisfy  $\int d^3\mathbf{r} \Psi^\dagger \Psi = N$ , the particle density of each component reads  $n_{m=1,0,-1} = |\Psi_m|^2$ , therefore the total particle density reads  $n = \sum_m n_m$ .  $\mathcal{F} = (\mathcal{F}_x, \mathcal{F}_y, \mathcal{F}_z)^T$  expresses a vector of spin-1 matrices. The optical trapping potential  $V_{opt}(\mathbf{r}) = m[\omega_r^2(x^2 + y^2) + \omega_z^2 z^2]/2$  is considered, where  $\omega_r$  and  $\omega_z$  are the radial and axial trapping frequencies,  $m$  is mass of <sup>87</sup>Rb atoms, the mass of a atom is given as  $m = 1.44 \times 10^{-25} kg$ . For the SO coupling term, it can be written as  $\mathcal{V}_{so} = -i\hbar(\kappa_x \mathcal{F}_x \partial_x + \kappa_y \mathcal{F}_y \partial_y)$ , where  $\mathcal{F}_{x,y}$  are the spin-1 matrices and  $\kappa_{x,y}$  denote the strength of SO coupling related to the strength of the magnetic pulses<sup>39</sup>. When  $\kappa_x = \kappa_y = \kappa$ , SO coupling reduces the isotropic Rashba type. In fact, we also consider the anisotropic SO

coupling  $\kappa_x \neq \kappa_y$ . The external magnetic field, which is a combination of two quadrupole fields<sup>18</sup>, can be written as  $\mathbf{B}(\mathbf{r}) = B'_1(x\hat{e}_x + y\hat{e}_y) + B'_2z\hat{e}_z$ , where Maxwell's equation  $\nabla \cdot \mathbf{B} = 0$ , so a condition is satisfied  $2B'_1 + B'_2 = 0$ . Where  $\mu_B$  is the Bohr magneton and the Landé factor  $g_F = -1/2$  for rubidium atoms. For the interaction terms, the coupling parameters are given by  $c_0 = 4\pi\hbar^2(a_0 + 2a_2)/3m$  and  $c_2 = 4\pi\hbar^2(a_2 - a_0)/3m$ , where  $a_f$  is s-wave scattering length for total hyperfine spin  $f$ . We consider the spinor BEC of <sup>87</sup>Rb atoms with ferromagnetic spin-spin interactions ( $c_2 < 0$ )<sup>8,64</sup>, the scattering for <sup>87</sup>Rb are  $a_2 = (100.4 \pm 0.1)a_B$  (total spin channel  $F_{total} = 2$ ) and  $a_0 = (101.8 \pm 0.2)a_B$  (total spin channel  $F_{total} = 0$ )<sup>65,66</sup>, where  $a_B$  is the Bohr radius.

The wave function of Bose-Einstein condensates satisfies the dimensionless coupled Gross-Pitaevskii (GP) equation<sup>42-44,57</sup>

$$i\frac{\partial\psi_1}{\partial t} = \left(-\frac{1}{2}\nabla^2 + V + \lambda_0\rho + \lambda_2(\rho_1 + \rho_0 - \rho_{-1}) + B_2z\right)\psi_1 + B_1(x - iy)\psi_0 + \kappa(-i\partial_x - \partial_y)\psi_0 + \lambda_2\psi_{-1}^*\psi_0^2, \quad (2)$$

$$i\frac{\partial\psi_0}{\partial t} = \left(-\frac{1}{2}\nabla^2 + V + \lambda_0\rho + \lambda_2(\rho_1 + \rho_{-1})\right)\psi_0 + B_1(x + iy)\psi_1 + B_1(x - iy)\psi_{-1} + \kappa(-i\partial_x + \partial_y)\psi_1 + \kappa(-i\partial_x - \partial_y)\psi_{-1} + 2\lambda_2\psi_1\psi_{-1}\psi_0^*, \quad (3)$$

$$i\frac{\partial\psi_{-1}}{\partial t} = \left(-\frac{1}{2}\nabla^2 + V + \lambda_0\rho + \lambda_2(\rho_0 + \rho_{-1} - \rho_1) - B_2z\right)\psi_{-1} + B_1(x + iy)\psi_0 + \kappa(-i\partial_x + \partial_y)\psi_0 + \lambda_2\psi_1^*\psi_0^2, \quad (4)$$

where the dimensionless wave functions  $\psi_j = \psi_j(\mathbf{r})(j = 1, 0, -1)$ ,  $\rho = \rho_1 + \rho_0 + \rho_{-1}$  is the total condensate density with  $\rho_j = |\psi_j|^2(j = 1, 0, -1)$ . Here, we introduce dimensionless pa-

parameter related to the coupled GP equation. The dimensionless wave functions is given as  $\psi_j = N^{-1/2} a_h^{3/2} \Psi_j (j = 1, 0, -1)$ , the condensate length is scaled in units of  $a_h = \sqrt{\hbar/m\omega}$ ,  $a_h$  is the characteristic length of the harmonic trap. The time by  $\omega^{-1}$ , the energy by  $\hbar\omega$ , and strength of SO coupling by  $\sqrt{\hbar\omega/m}$ . The dimensionless optical trapping potential  $V(\mathbf{r}) = \frac{1}{2}(\gamma_r^2 x^2 + \gamma_r^2 y^2 + \gamma_z^2 z^2)$  with  $\gamma_r = \omega_r/\omega, \gamma_z = \omega_z/\omega$ , and  $\omega = \min\{\omega_r, \omega_z\}$ . The interaction strengths  $\lambda_0$  and  $\lambda_2$ , which determined the scattering length  $a_f$  and the number of particles  $N$ . The strength of magnetic field gradient is given in the units of  $(g_F \mu_B a_h)/\omega \hbar$ . In the simulation, the minimum-energy density and phase distributions of Dirac monopoles are solved from Eq.(3) - Eq.(5), the standard imaginary-time propagation combined with second-order centered finite-difference discretization and backward/forward Euler methods are used<sup>61-63</sup>, and the periodic boundary conditions are considered. The volume in our calculation is  $20 \times 20 \times 20$  in the units of  $a_h^3$ , the computational grid consists of  $120 \times 120 \times 120$  points.

**The monopoles attached to the polar-core vortex induced by weak spin-orbit coupling.** We observe different stationary states of Dirac monopoles in the presence of the weak Rashba SO coupling. In this simulation, the quadrupole field gradient strength is considered  $B_1 = 0.6$ , the isotropic optical trap potential of  $\omega_r = \omega_z = 2\pi \times 250$  Hz is considered<sup>18</sup>. First of all, we find similar to metastable monopole in the absence of Rashba SO coupling, the results from this simulation are shown in Figs. 2(a1)-2(a3). Fig. 2(a1) illustrates density isosurfaces of the three spin components of monopoles. Fig. 2(a2) shows the local density isosurfaces with the slice planes the corresponding each spin component. Specifically, the slice plane is  $z = -3.5$  for spin state  $m_F = 1$ , the slice planes are  $z = 3.5$  and  $y = 3.5$  for spin state  $m_F = 0$ , the slice plane is



$z = 3.5$  for spin state  $m_F = -1$ . We find that a point singularity is attached to a vortex line singularity, as a result, the vortex line may be closed inside of the atomic cloud, or terminated at the boundary of the atomic cloud. In physics, the singular vortex line is called Dirac string<sup>3,8,18</sup>. For spin state  $m_F = 1$ , we can find that vortex lines along the negative  $z$  axis, the one reaches the boundary of Bose-Einstein condensates along the positive  $y$  axis, and the other one reaches the boundary of Bose-Einstein condensates along the negative  $y$  axis. Note that for  $z > 0$  there are no line singularities. For spin state  $m_F = 0$ , an interesting result shows two strings in the  $x = 0$  plane to cross each other, the similar phenomenon was predicted in previous work<sup>25</sup>. For spin state  $m_F = -1$ , the Dirac strings are along the positive  $z$  axis, the rest of the phenomenon is the same as  $m_F = 1$  component. Fig. 2(a3) shows the phase distribution in the corresponding slice plane of each component. In detail, in the absence of SO coupling, we observe that a Dirac string with a doubly quantized vortex splits into two strings with a singly quantized vortex, it is important that the phases of both sides in the case of the vortex line are inverse. Topologically invariant winding number is just one for  $m_F = 0$  component, but the phase of the vortex line along the  $z$  axis and  $y$  axis is opposed, similar to a vortex-antivortex pair<sup>67,68</sup>. Our results are similar to the monopole states that have been studied previously<sup>8,22</sup>. In fact, when the time evolution as long as possible is considered, it is natural that these doubly quantized vortices split into two singly quantized vortices<sup>69,70</sup>, hence our results can be known as the metastable monopole states.

Next, the weak Rashba SO coupling is considered, it is found that the weak Rashba SO coupling induces two kinds of the monopole states. First of all, we observe that SO coupling induces the monopole state of polar-core vortex<sup>52</sup>, here, the strength of SO coupling  $\kappa = 2$ , the spin-

dependent interaction coefficient  $\lambda_2 = -75$ . The results from this simulation are illustrated in Figs. 2(b1)-2(b3). Fig. 2(b1) illustrates density isosurfaces of the three spin components of the monopoles, Fig. 2(b2) shows the local density isosurfaces with the slice planes the corresponding each spin component, where the slice plane is  $z = 0$  for all the spin states. Fig. 2(b3) displays the phase distribution with respect to the three spin components. In detail, the structure of the monopole with polar-core vortex in terms of every spin components is as follows: a singly vortex line in the  $m_F = 1$  component, a singly antivortex line in the  $m_F = -1$  component, and a soliton in the  $m_F = 0$  component. In addition, we can obtain that the phases of both sides belong to the slice plane of  $x = 0$  and  $y = 0$  are inverse. It is reported that the polar-core vortex is stable in the ferromagnetic and antiferromagnetic Bose-Einstein condensates<sup>54</sup>, indeed, the SO coupling leads to the stable magnetic monopole. When the strength of SO coupling  $\kappa = 2$ , the spin-dependent interaction coefficient  $\lambda_2 = -15$ , we find that SO coupling gives rise to the monopole state of Mermin-Ho vortex<sup>55</sup>. It is obtained that the Mermin-Ho vortex is stable and robust in the ferromagnetic spinor Bose-Einstein condensates<sup>55</sup>. The results from this simulation are indicated in Figs. 2(c1)-2(c3). Fig. 2(c1) illustrates density isosurfaces of the three spin components of monopoles, Fig. 2(c2) displays the local density isosurfaces with the slice planes the corresponding each spin component, where the slice plane is also  $z = 0$  for all the spin states. Fig. 2(c3) displays the phase distribution with respect to the three spin components. In detail, the structure of the monopole with Mermin-Ho vortex in terms of every spin components is as follows: a soliton in the  $m_F = 1$  component, a singly vortex line in the  $m_F = 0$  component, and a doubly quantized vortex line in the  $m_F = -1$  component, the phase winding direction is same for both  $m_F = 0$  and

$m_F = -1$  component, in addition, we also obtain that both sides phases belong to the slice plane of  $x = 0$  and  $y = 0$  are inverse.

**The square lattice state of monopoles induced by strong spin-orbit coupling.** For the fixed values of the spin-independent as well as spin-dependent interaction, we observe the monopoles states transformation from polar-core vortex state to square lattice state as increasing SO coupling strength. Obviously, when the SO coupling is weak, in other words, the strength of SO coupling  $\kappa = 2$ , the monopole state behaves as polar-core vortex. In detail, Figs. 3(a1)-3(b1) display the density distribution of each spin component for  $x \leq 0$  and  $z \leq 0$ . Figs. 3(a2)-3(b2) indicate the phase distribution of each spin component for the slice planes with  $x = 0$  and  $z = 0$ . When the strong SO coupling strength  $\kappa = 16$ , the square lattice state emerges in the system. Figs. 3(c1)-3(d1) display the density distribution of each spin component for  $x \leq 0$  and  $z \leq 0$ , Figs. 3(c2)-3(d2) indicate the phase distribution of each spin component for the slice planes with  $x = 0$  and  $z = 0$ . We observe that the condensate density divides into four quadrants in x-y plane, particularly, the square lattice is extraordinary distinct in the central zone of Bose-Einstein condensates, meanwhile, the density distribution of its longitudinal direction similar to stripe structure, moreover, both sides phases belong to the slice plane of  $x = 0$  are inverse for all components. On the other hand, monopoles and antimonopoles emerge in the square lattice state.

We also consider the monopole state under the anisotropic SO coupling, here, the strength of SO coupling along x axis  $\kappa_x = 8$ , the strength of SO coupling along y axis  $\kappa_y = 2$ , other parameters are same as Fig. 3. The results in the case of the anisotropic SO coupling are shown in Fig. 4,

Fig. 4(a) illustrates density isosurfaces, the density and phase distribution the corresponding slice plane of  $z = 0$  and  $x = 0$  for the  $m_F = 1$  component. Fig. 4(b) illustrates density isosurfaces, the density and phase distribution the corresponding slice plane of  $z = 0$  and  $x = 0$  for the  $m_F = 0$  component. Fig. 4(c) illustrates density isosurfaces, the density and phase distribution the corresponding slice plane of  $z = 0$  and  $x = 0$  for the  $m_F = -1$  component. Our result shows the monopole vanishes under the anisotropic SO coupling, in addition, we can observe that the condensate splits into many segments along the x direction, such a density modulation can be understood as a stripe phase along the x direction induced by the anisotropic SO coupling, the density distribution in y-z plane can be considered as plane wave phase.

**Spin textures of the monopoles.** We demonstrate that topologically spin textures of magnetic monopoles, the components of the spin vector are given by<sup>43,44,52,55,58-60</sup>

$$\begin{aligned}
F_x &= \frac{1}{\sqrt{2}}[\psi_1^* \psi_0 + \psi_0^*(\psi_1 + \psi_{-1}) + \psi_{-1}^* \psi_0], \\
F_y &= \frac{i}{\sqrt{2}}[-\psi_1^* \psi_0 + \psi_0^*(\psi_1 - \psi_{-1}) + \psi_{-1}^* \psi_0], \\
F_z &= |\psi_1|^2 - |\psi_{-1}|^2,
\end{aligned} \tag{5}$$

Fig. 5 indicates the spin textures of the monopole for slice planes with  $z = 5$ ,  $y = 5$  and  $x = 5$ , respectively. In Fig. 5(a), the SO coupling strength  $\kappa = 2$ , note that these textures behave as the coreless textures, similar the textures have been studied in the rotating spinor Bose-Einstein condensates<sup>52</sup>. Our result indicates the spin aligns with the radially inward hedgehog distribution in the  $F_x$ - $F_y$  plane, indeed, such the result suggests the spin texture of a south magnetic pole. Moreover, the textures with respect to the  $F_x$ - $F_z$  and  $F_y$ - $F_z$  planes form the cross hyperbolic distribution, such cross-disgyration spin texture is also called the mixed-twist texture<sup>53</sup>. Fig. 5(b) shows

the spin textures of the monopole in the case of strong SO coupling, here, the SO coupling strength  $\kappa = 16$ , we observe that the textures distribution include four portions in the  $F_x$ - $F_y$  plane. The texture of every portion behaves as the plane wave ferromagnet, and the spin orientations along the diagonal line are opposite. In fact, such these spin orientations behave as the structures of monopoles and antimonopoles, locating in the boundary of the condensate. Additionally, the textures with respect to the  $F_x$ - $F_z$  and  $F_y$ - $F_z$  planes form the spin stripe. In Fig. 5(c), the anisotropic SO coupling  $\kappa_x = 8$  and  $\kappa_y = 2$ , we can find the spin stripe texture in the  $F_x$ - $F_y$  and  $F_x$ - $F_z$  planes, the spin texture to  $F_y$ - $F_z$  plane seem as plane wave distribution. The colors ranging from blue to red represent the values of spin component.

**Phase diagrams of the monopoles.** We have obtained the phase diagrams by solving Eq. (3)-Eq. (5) for a large number of parameter values, which consist of SO coupling strength  $\kappa$ , spin-dependent interaction constant  $\lambda_2$ , and spin-independent interaction constant  $\lambda_0$ , all the results are summarized in Fig. 6. The phase diagram with respect to  $\kappa$  and  $\lambda_0$  values is illustrated in Fig. 6(a), here, the fixed spin-dependent interaction  $\lambda_2 = -75$ , there is the metastable monopole when SO coupling below a critical value  $\kappa_c = 0.8$  for the arbitrary  $\lambda_0$ . When  $\kappa$  increases ( $0.8 < \kappa \leq 3$ ), two kinds of vortex phase the corresponding the monopole emerges alternately, more precisely to say, Dirac monopoles accompanied with polar-core vortex can occur for  $0 < \lambda_0 \leq 3000$  and  $5000 < \lambda_0 \leq 8000$ . Dirac monopoles accompanied with Mermin-Ho vortex can occur for  $3000 < \lambda_0 \leq 5000$  and  $8000 < \lambda_0 \leq 11000$ . In addition, when  $\kappa > 3$ , there is also a direct vortex phase to square lattice phase transition for the arbitrary  $\lambda_0$ . In this case, our result suggests a cyclic phase transition from Dirac monopoles attached to polar-core vortex to that attached to Mermin-Ho

vortex can occur by varying the strength of two-body interaction. The phase diagram with respect to  $\kappa$  and  $\lambda_2$  values is plotted in Fig. 6(b), here, spin-independent interaction constant  $\lambda_0 = 7500$ , the metastable monopole can occur when SO coupling below a critical value  $\kappa_c = 0.8$  for the arbitrary  $\lambda_2$ . When SO coupling is satisfied  $0.8 < \kappa \leq 3$ , two kinds of vortex states the corresponding the monopole can emerge, spin-dependent interaction below the border value  $\lambda_2 = -30$ , the polar-core vortex phase the corresponding the monopole is observed. Moreover, spin-dependent interaction exceed the border value  $\lambda_2 = -30$ , the Mermin-Ho vortex phase the corresponding the monopole is found, further, when SO coupling is above a critical value  $\kappa_c = 3$ , there is a direct vortex phase to square lattice phase transition for the arbitrary  $\lambda_2$ .

## Discussion

We demonstrate Dirac monopoles attached to polar-core vortex induced by weak SO coupling in ferromagnetic Bose-Einstein condensates. We find a cyclic phase transition from Dirac monopoles with polar-core vortex to that with Mermin-Ho vortex induced by SO coupling. In detail, for very weak limit SO coupling ( $\kappa \leq 0.8$ ), the result shows the monopole state the corresponding vortex structures of two strings similar to the nonaxisymmetric vortices<sup>54</sup>. Such vortices are proved that their stabilities are restricted in a very narrow parameter region, in this case, the result suggests the monopole state maybe is the metastable. On the other hand, our study suggests two types of monopoles with the polar-core vortex and Mermin-Ho vortex under the weak SO coupling ( $0.8 < \kappa \leq 3$ ), these two types of vortices also are viewed as the axisymmetric vortices<sup>54</sup>. As we known, the axisymmetric vortices are more stable than the nonaxisymmetric vortices, hence, our

result suggests the possible conditions that the monopole can be stable for the weak SO coupling ( $0.8 < \kappa \leq 3$ ). Meanwhile, it is notable that such two types of monopoles can occur phase transition each other within the parameter region. In addition, for large enough SO coupling, we observed the square lattice phase, note that the emergence of the square lattice phase not be affected by spin-dependent interactions and spin-independent interactions. More precisely speaking, our study indicates that the square lattice state for x-y plane and the stripe state for both x-z plane and y-z plane. The square lattice state of two dimension has also been predicted in rapidly quenched spin-orbit coupled spinor Bose-Einstein condensates<sup>43</sup>. In the present work, we also find that the monopole vanishes under the anisotropic SO coupling, whereas the stripe phase emerges.

To summarize, we have investigated the phase diagrams and exotic phase transitions of monopoles in SO coupled spinor Bose-Einstein condensates. We also show how the strong and anisotropic SO coupling modify the monopoles states. Our results different from the previous conclusions of monopoles in spinor Bose-Einstein condensates without SO coupling, beyond the previous investigations. In particular, such these monopoles can be proved by means of imaging the vortex lines in experiment, hence, the monopoles can be detected by the time-of-flight absorption imaging technique in a real experiment. This work opens a new window to realize complex nontrivial topological structure of the monopole with respect to gauge field in future experiments and theories.

## Methods

**Calculation of stationary states with respect to monopoles.** We investigate the stationary state of the monopole in SO coupled spinor Bose-Einstein condensates, which based on the Gross-Pitaevskii mean-field theory. We can obtain the stationary state wave function of the monopole with the help of the standard imaginary-time propagation. Specifically speaking, in solving the time evolution equations, first of all, we can obtain an imaginary time by applying the transformation relation expressed as  $t \rightarrow -it$ , as a result, the imaginary time evolution equations are expressed as follows:

$$\begin{aligned} \frac{\partial \psi_1}{\partial t} = & \left( \frac{1}{2} \nabla^2 - V - \lambda_0 \rho - \lambda_2 (\rho_1 + \rho_0 - \rho_{-1}) - B_2 z \right) \psi_1 \\ & - B_1 (x - iy) \psi_0 - \kappa (-i \partial_x - \partial_y) \psi_0 - \lambda_2 \psi_{-1}^* \psi_0^2, \end{aligned} \quad (6)$$

$$\begin{aligned} \frac{\partial \psi_0}{\partial t} = & \left( \frac{1}{2} \nabla^2 - V - \lambda_0 \rho - \lambda_2 (\rho_1 + \rho_{-1}) \right) \psi_0 \\ & - B_1 (x + iy) \psi_1 - B_1 (x - iy) \psi_{-1} - \kappa (-i \partial_x + \partial_y) \psi_1 \\ & - \kappa (-i \partial_x - \partial_y) \psi_{-1} - 2 \lambda_2 \psi_1 \psi_{-1} \psi_0^*, \end{aligned} \quad (7)$$

$$\begin{aligned} \frac{\partial \psi_{-1}}{\partial t} = & \left( \frac{1}{2} \nabla^2 - V - \lambda_0 \rho - \lambda_2 (\rho_0 + \rho_{-1} - \rho_1) + B_2 z \right) \psi_{-1} \\ & - B_1 (x + iy) \psi_0 - \kappa (-i \partial_x + \partial_y) \psi_0 - \lambda_2 \psi_1^* \psi_0^2, \end{aligned} \quad (8)$$

where the dimensionless wave functions  $\psi_j = \psi_j(\mathbf{r})$  ( $j = 1, 0, -1$ ),  $\rho = \rho_1 + \rho_0 + \rho_{-1}$  is the total condensate density with  $\rho_j = |\psi_j|^2$  ( $j = 1, 0, -1$ ). The strength of SO coupling is given in the units of  $\sqrt{\hbar \omega / m}$ , the dimensionless optical trapping potential  $V(\mathbf{r}) = \frac{1}{2}(\gamma_r^2 x^2 + \gamma_r^2 y^2 + \gamma_z^2 z^2)$  with  $\gamma_r = \omega_r / \omega$ ,  $\gamma_z = \omega_z / \omega$ , and  $\omega = \min\{\omega_r, \omega_z\}$ . The interaction strengths  $\lambda_0$  and  $\lambda_2$ , which



determined the scattering length  $a_f$  and the number of particles  $N$ , the strength of magnetic field gradient is given in the units of  $(g_F \mu_B a_h) / \omega \hbar$ . In addition, the average energy of the system is expressed as follows:

$$\begin{aligned}
E(\psi_1, \psi_0, \psi_{-1}) = \int_{\Omega} \left\{ \sum_{m=0, \pm 1} \psi_m^* h_d \psi_m + \frac{\lambda_0}{2} \rho^2 + \frac{\lambda_2}{2} (\rho_1 + \rho_0 - \rho_{-1}) \rho_1 \right. \\
+ \frac{\lambda_2}{2} (\rho_1 + \rho_{-1}) \rho_0 + \frac{\lambda_2}{2} (\rho_0 + \rho_{-1} - \rho_1) \rho_{-1} \\
+ \lambda_2 (\psi_{-1}^* \psi_0^2 \psi_1^* + \psi_{-1} \psi_0^{*2} \psi_1) + B_2 z (\rho_1 - \rho_{-1}) \\
+ B_1 (x - iy) (\psi_1^* \psi_0 + \psi_0^* \psi_{-1}) + B_1 (x + iy) (\psi_0^* \psi_1 + \psi_{-1}^* \psi_0) \\
+ \kappa [\psi_1^* (-i\partial_x - \partial_y) \psi_0 + \psi_0^* (-i\partial_x + \partial_y) \psi_1 \\
\left. + \psi_0^* (-i\partial_x - \partial_y) \psi_{-1} + \psi_{-1}^* (-i\partial_x + \partial_y) \psi_0 \right\} d\Omega, \tag{9}
\end{aligned}$$

for the spatial discretization, we take second-order centered finite-difference for spatial derivatives. For the time discretization, we use the backward/forward Euler scheme for linear/nonlinear terms in time derivatives. The periodic boundary conditions are considered, the volume in our calculation is  $20 \times 20 \times 20$  in the units of  $a_h^3$ , the computational grid consists of  $120 \times 120 \times 120$  points. In order to get the final steady state, an initial trial state given is necessary. In this work, the final steady state is not depend on the initial trial wave function, here, we choose the normalized random number of complex-valued. As we known, the average energy decays monotonically in time as far as the steady states are reached.

1. Dirac, P. A. M. Quantised singularities in the electromagnetic field. *Proc. R. Soc. A.* **133**, 60 (1931).
2. Castelnovo, C., Moessner, R. & Sondhi, S. L. Magnetic monopoles in spin ice. *Nature* **451**, 42

- (2008).
3. Morris, D. J. P. *et al.* Dirac strings and magnetic monopoles in the spin ice  $Dy_2Ti_2O_7$ . *Science* **326**, 411 (2009).
  4. Pollard, S. D., Volkov, V. & Zhu, Y. Propagation of magnetic charge monopoles and Dirac flux strings in an artificial spin-ice lattice. *Phys. Rev. B* **85**, 180402(R) (2012).
  5. Zhou, H. D., Bramwell, S. T., Cheng, J. G., Wiebe, C. R., Li, G., Balicas, L., Bloxson, J. A., Silverstein, H. J., Zhou, J. S., Goodenough, J. B., & Gardner, J. S. High pressure route to generate magnetic monopole dimers in spin ice. *Nat. Commun.* **2**, 478 (2011).
  6. Khomskii, D. I. Electric dipoles on magnetic monopoles in spin ice. *Nat. Commun.* **3**, 904 (2012).
  7. Bovo, L., Bloxson, J. A., Prabhakaran, D., Aeppli, G., & Bramwell, S. T. Brownian motion and quantum dynamics of magnetic monopoles in spin ice. *Nat. Commun.* **4**, 1535 (2013).
  8. Ray, M. W., Ruokokoski, E., Kandel, S., Möttönen, M. & Hall, D. S. Observation of Dirac monopoles in a synthetic magnetic field. *Nature (London)* **505**, 657 (2014).
  9. Ray, M. W., Ruokokoski, E., Tiurev, K., Möttönen, M. & Hall, D. S. Observation of isolated monopoles in a quantum field. *Science* **348**, 544 (2015).
  10. Cardoso, M., Bicudo, P. & Sacramento, P. D. Confinement of monopole field lines in a superconductors at  $t \neq 0$ . *Ann. Phys.* **323**, 337 (2008).

11. Goddard, P. & Olive, D. I. Magnetic monopoles in gauge field theories. *Rep. Prog. Phys.* **41**, 1357 (1978).
12. Brekke, L., Fischler, W. & Imbo, T. D. Alice strings, magnetic monopoles, and charge quantization. *Phys. Rev. Lett.* **67**, 3643 (1991).
13. Bakker, B. L. G., Chernodub, M. N. & Polikarpov, M. I. Abelian monopoles in SU(2) lattice gauge theory as physical objects. *Phys. Rev. Lett.* **80**, 30 (1998).
14. Williams, J. E. & Holland, M. J. Preparing topological states of a Bose-Einstein condensate. *Nature* **401**, 568 (1999).
15. Khawaja, U. A. & Stoof, H. Skyrmions in a ferromagnetic Bose-Einstein condensate. *Nature* **411**, 918 (2001).
16. Choi, J. -y., Kwon, W. J. & Shin, Y. -i. Observation of topologically stable 2D skyrmions in an antiferromagnetic spinor Bose-Einstein condensate. *Phys. Rev. Lett.* **108**, 035301 (2012).
17. Martikainen, J. -P., Collin, A. & Suominen, K. -A. Creation of a monopole in a spinor condensate. *Phys. Rev. Lett.* **88**, 090404 (2002).
18. Pietilä, V. & Möttönen, M. Creation of Dirac monopoles in Spinor Bose-Einstein Condensates. *Phys. Rev. Lett.* **103**, 030401 (2009).
19. Busch, Th. & Anglin, J R. Wave-function monopoles in Bose-Einstein condensates. *Phys. Rev. A* **60**, R2669 (1999).

20. García-Ripoll, J. J. *et al.* Spin monopoles with Bose-Einstein condensates. *Phys. Rev. A* **61**, 053609 (2000).
21. Stoof, H. T. C., Vliegen, E. & Al Khawaja, U. Monopoles in an antiferromagnetic Bose-Einstein condensate. *Phys. Rev. Lett.* **87**, 120407 (2001).
22. Savage, C. M. & Ruostekoski, J. Dirac monopoles and dipoles in ferromagnetic spinor Bose-Einstein condensates. *Phys. Rev. A* **68**, 034604 (2003).
23. Ruokokoski, E., Pietilä, V. & Möttönen, M. Ground-state Dirac monopole. *Phys. Rev. A* **84**, 063627 (2011).
24. Pietilä, V. & Möttönen, M. Non-abelian magnetic monopole in a Bose-Einstein condensate. *Phys. Rev. Lett.* **102**, 080403 (2009).
25. Conduit, G. J. Line of Dirac monopoles embedded in a Bose-Einstein condensate. *Phys. Rev. A* **86**, 021605(R) (2012).
26. Cho, Y. M. Monopoles and knots in skyrme theory. *Phys. Rev. Lett.* **87**, 252001 (2001).
27. Solnyshkov, D. D., Flayac, H. & Malpuech, G. Stable magnetic monopoles in spinor polariton condensates. *Phys. Rev. B* **85**, 073105 (2012).
28. Kiffner, M., Li, W. H. & Jaksch, D. Magnetic monopoles and synthetic spin-orbit coupling in rydberg macrodimers. *Phys. Rev. Lett.* **110**, 170402 (2013).
29. Bernevig, B. A., Hughes, T. L. & Zhang, S. C. Quantum spin Hall effect and topological phase transition in HgTe quantum wells. *Science* **314**, 1757 (2006).

30. König, M., Wiedmann, S., Brüne, C., Roth, A., Buhmann, H., Molenkamp, L. M., Qi, X. L. & Zhang, S. C. Quantum spin hall insulator state in HgTe quantum wells. *Science* **318**, 766 (2007).
31. Lin, Y. J., Jiménez-García, K. & Spielman, I. B. Spin-orbit-coupled Bose-Einstein condensates. *Nature (London)* **471**, 83 (2011).
32. Ruseckas, J., Juzeliūnas, G., Öhberg, P. & Fleischhauer, M. Non-abelian gauge potentials for ultracold atoms with degenerate dark states. *Phys. Rev. Lett.* **95**, 010404 (2005).
33. Liu, X. J., Borunda, M. F., Liu, X. & Sinova, J. Effect of induced spin-orbit coupling for atoms via laser fields. *Phys. Rev. Lett.* **102**, 046402 (2009).
34. Zhang, J. Y., Ji, S. C., Chen, Z., Zhang, L., Du, Z. D., Yan, B., Pan, G. S., Zhao, B., Deng, Y. J., Zhai, H., Chen, S. & Pan, J. W. Collective dipole oscillations of a Spin-Orbit Coupled Bose-Einstein Condensate. *Phys. Rev. Lett.* **109**, 115301 (2012).
35. Ji, S. C., Zhang, J. Y., Zhang, L., Du, Z. D., Zheng, W., Deng, Y. J., Zhai, H., Chen, S. & Pan, J. W. Experimental determination of the finite-temperature phase diagram of a spin-orbit coupled Bose gas. *Nat. Phys.* **10**, 314 (2014).
36. Campbell, D. L., Juzeliūnas, G. & Spielman, I. B. Realistic Rashba and Dresselhaus spin-orbit coupling for neutral atoms. *Phys. Rev. A* **84**, 025602 (2011).
37. Lan, Z. H. & Öhberg, P. Raman-dressed spin-1 spin-orbit-coupled quantum gas. *Phys. Rev. A* **89**, 023630 (2014).

38. Anderson, B. M., Juzeliūnas, G., Galitski, V. M. & Spielman, I. B. Synthetic 3D spin-orbit coupling. *Phys. Rev. Lett.* **108**, 253301 (2012).
39. Anderson, B. M., Spielman, I. B. & Juzeliūnas, G. Magnetically generated Spin-Orbit Coupling for ultracold atoms. *Phys. Rev. Lett.* **111**, 125301 (2013).
40. Wang, P. J., Yu, Z. Q., Fu, Z. K., Miao, J., Huang, L. H., Chai, S. J., Zhai, H. & Zhang, J. Spin-orbit coupled degenerate Fermi gases. *Phys. Rev. Lett.* **109**, 095301 (2012).
41. Cheuk, L. W., Sommer, A. T., Hadzibabic, Z., Yefsah, T., Bakr, W. S. & Zwierlein, M. W. Spin-injection spectroscopy of a spin-orbit coupled fermi gas. *Phys. Rev. Lett.* **109**, 095302 (2012).
42. Wang, C. J., Gao, C., Jian, C. M. & Zhai, H. Spin-Orbit Coupled Spinor Bose-Einstein Condensates. *Phys. Rev. Lett.* **105**, 160403 (2010).
43. Su, S. W., Liu, I. K., Tsai, Y. C., Liu, W. M. & Gou, S. C. Crystallized half-skyrmions and inverted half-skyrmions in the condensation of spin-1 Bose gases with spin-orbit coupling. *Phys. Rev. A* **86**, 023601 (2012).
44. Liu, C. F. & Liu, W. M. Spin-orbit-coupling-induced half-skyrmion excitations in rotating and rapidly quenched spin-1 Bose-Einstein condensates. *Phys. Rev. A* **86**, 033602 (2012).
45. Xu, X. Q. & Han, J. H. Spin-orbit coupled Bose-Einstein condensate under rotation. *Phys. Rev. Lett.* **107**, 200401 (2011).

46. Sinha, S., Nath, R. & Santos, L. Trapped two-dimensional condensates with synthetic spin-orbit coupling. *Phys. Rev. Lett.* **107**, 270401 (2011).
47. Hu, H., Ramachandhran, B. & Liu, X. J. Spin-orbit coupled weakly interacting Bose-Einstein condensates in harmonic traps. *Phys. Rev. Lett.* **108**, 010402 (2012).
48. Gopalakrishnan, S., Martin, I. & Demler, E. A. Quantum quasicrystals of spin-orbit-coupled dipolar bosons. *Phys. Rev. Lett.* **111**, 185304 (2013).
49. Li, Y., Martone, G. I., Pitaevskii, L. P. & Stringari, S. Superstripes and the excitation spectrum of a spin-orbit-coupled Bose-Einstein condensate. *Phys. Rev. Lett.* **110**, 235302 (2013).
50. Han, W., Juzeliūnas, G., Zhang, W. & Liu, W. M. Supersolid with nontrivial topological spin textures in spin-orbit-coupled Bose gases. *Phys. Rev. A* **91**, 013607 (2015).
51. Kawaguchi, Y., Nitta, M. & Ueda, M. Knots in a spinor Bose-Einstein Condensates. *Phys. Rev. Lett.* **100**, 180403 (2008).
52. Mizushima, T., Kobayashi, N. & Machida, K. Coreless and singular vortex lattices in rotating Spinor Bose-Einstein Condensates. *Phys. Rev. A* **70**, 043613 (2004).
53. Kita, T. Vortex-lattice phases of superfluid  $^3\text{He}$  in rapid rotation. *Phys. Rev. Lett.* **86**, 834 (2001).
54. Mizushima, T., Machida, K. & Kita, T. Axisymmetric versus nonaxisymmetric vortices in Spinor Bose-Einstein Condensates. *Phys. Rev. A* **66**, 053610 (2002).

55. Mizushima, T., Machida, K. & Kita, T. Mermin-Ho vortex in ferromagnetic Spinor Bose-Einstein Condensates. *Phys. Rev. Lett.* **89**, 030401 (2002).
56. Ho, T. L. Spinor Bose condensates in optical traps. *Phys. Rev. Lett.* **81**, 742 (1998).
57. Pu, H., Law, C. K., Raghavan, S., Eberly, J. H. & Bigelow, N. P. Spin-mixing dynamics of a spinor Bose-Einstein condensate. *Phys. Rev. A* **60**, 1463 (1999).
58. Kasamatsu, K., Tsubota, M. & Ueda, M. Vortex molecules in coherently coupled two-component Bose-Einstein Condensates. *Phys. Rev. Lett.* **93**, 250406 (2004).
59. Kawakami, T., Mizushima, T., Nitta, M. & Machida, K. Stable skyrmions in SU(2) gauged Bose-Einstein Condensates. *Phys. Rev. Lett.* **109**, 015301 (2012).
60. Kasamatsu, K., Tsubota, M. & Ueda, M. Spin textures in rotating two-component Bose-Einstein Condensates. *Phys. Rev. A* **71**, 043611 (2005).
61. Dalfovo, F. & Stringari, S. Bosons in anisotropic traps: Ground state and vortices. *Phys. Rev. A* **53**, 2477 (1996).
62. Zhang, X. F., Dong, R. F., Liu, T., Liu, W. M. & Zhang, S. G. Spin-orbit-coupled Bose-Einstein condensates confined in concentric coupled annular traps. *Phys. Rev. A* **86**, 063628 (2012).
63. Bao, W. Z. & Du, Q. Computing the ground state solution of Bose-Einstein condensates by a normalized gradient flow. *SIAM J. Sci. Comput.* **25**, 1674 (2004).
64. Stenger, J., Inouye, S., Stamper-Kurn, D. M., Miesner, H. -J., Chikkatur, A. P. & Ketterle, W. Spin domains in ground-state Bose-Einstein condensates. *Nature (London)* **396**, 345 (1998).



65. van Kempen, E. G. M., Kokkelmans, S. J. J. M. F., Heinzen, D. J. & Verhaar, B. J. Interisotope determination of ultracold rubidium interactions from three high-precision experiments. *Phys. Rev. Lett.* **88**, 093201 (2002).
66. Stamper-Kurn, Dan M. & Ueda, M. Spinor Bose gases: Symmetries, magnetism, and quantum dynamics. *Revi. Mod. Phys.* **85**, 1191 (2013).
67. Devreese, J. P. A., Tempere, J. & Sá de Melo, Carlos A. R. Effects of Spin-Orbit Coupling on the Berezinskii-Kosterlitz-Thouless transition and the vortex-antivortex structure in two-dimensional Fermi gases. *Phys. Rev. Lett.* **113**, 165304 (2014).
68. Chibotaru, L. F., Ceulemans, A., Bruyndoncx, V. & Moshchalkov, V. V. Symmetry-induced formation of antivortices in mesoscopic superconductors. *Nature (London)* **408**, 833 (2000).
69. Shin, Y., Saba, M., Vengalattore, M., Pasquini, T. A., Sanner, C., Leanhardt, A. E., Prentiss, M., Pritchard, D. E. & Ketterle, W. Dynamical instability of a doubly quantized vortex in a Bose-Einstein Condensate. *Phys. Rev. Lett.* **93**, 160406 (2004).
70. Huhtamäki, J. A. M., Möttönen, M., Isoshima, T., Pietilä, V. & Virtanen, S. M. M. Splitting time of doubly quantized vortices in dilute Bose-Einstein Condensates. *Phys. Rev. Lett.* **97**, 110406 (2006).

**Acknowledgement** This work was supported by the NSFC under grants Nos. 11434015, 61227902, 61378017, NKBRSCF under grants Nos. 2012CB821305, SKLQQOD under grants No. KF201403, SPRPCAS under grants No. XDB01020300.

**Author Contributions** All authors planned and designed theoretical and numerical studies. All contributed in completing the paper.

**Competing Interests** The authors declare that they have no competing financial interests.

**Correspondence** Correspondence should be addressed to Liu, Wu-Ming (email: wliu@iphy.ac.cn).

**Figure 1 Experimental setup for creating spin-orbit coupling and the quadrupole field in spinor Bose-Einstein condensates.** (a) The experimental geometry of creating spin-orbit (SO) coupling via pulsed magnetic field, where the pink particles represent  $^{87}\text{Rb}$  atoms, the cloud of atoms is located  $50\mu\text{m}$  above the surface of an atom chip, a bias field  $B_0$  along  $z$  axis induces the magnetic splitting. Two pairs of parallel microwires are embedded in the atom chip, which produce the amplitude modulated rf field along  $x$  and  $y$  axis, respectively, these two effective coupling vectors in  $x$ - $y$  plane induce effective 2D SO coupling in the first-order approximation to short enough duration. (b) Schematic representation for creating the quadrupole field. A pair of Helmholtz coils are used for creating the quadrupole fields (Q), the inset displays the distribution of quadrupole magnetic field, where the pink particles represent Bose gases of  $^{87}\text{Rb}$  atoms, kermesinus arrows show beam paths of the optical trap. (c) Energy spectrum. The single-particle energy spectrum of the monopole with SO coupling strength  $\kappa = 2$  in  $k_x - k_y$  plane is divided into three branches  $E_+$ ,  $E_0$  and  $E_-$ , the black circular ring represents the Rashba ring from the minimum energy spectrum. (d) Spin distribution of the monopole, which is like the radially outward hedgehog form, the black dot shows the location of magnetic charge.

**Figure 2 The monopoles attached to the polar-core and Mermin-Ho vortex induced by spin-orbit coupling.** (a1-a3) The first column shows the isosurface of particle densities of each component on the monopole. The second column displays the bounded particle densities of each component on the monopole, where the slice plane of the first row is  $z = -3.5$  for spin state  $m_F = 1$ , the slice planes of the second row are  $z = 3.5$  and  $y = 3.5$  for spin state  $m_F = 0$ , the slice plane of the third row is  $z = 3.5$  for spin state  $m_F = -1$ . The third column shows

phase distributions the corresponding slice plane of each component. Here, the strength of spin-orbit (SO) coupling  $\kappa = 0$ , the spin-dependent interaction coefficient  $\lambda_2 = -75$ . **(b1-b3)** The fourth column shows the isosurface of particle densities of the monopole attached to the polar-core vortex. The fifth column displays the bounded particle densities of each component, where the slice planes are  $z = 0$  for all the spin states, the sixth column shows phase distributions of each component. The structure of the monopole is as follows: a singly vortex line in the  $m_F = 1$  component, a singly antivortex line in the  $m_F = -1$  component, and a soliton in the  $m_F = 0$  component. Here, the strength of SO coupling  $\kappa = 2$ , the spin-dependent interaction coefficient  $\lambda_2 = -75$ . **(c1-c3)** The seventh column shows the isosurface of particle densities of the monopole attached to the Mermin-Ho vortex, the eighth column displays the bounded particle densities for of each component, where the slice planes are  $z = 0$  for all the spin states, the ninth column shows phase distributions of each component. In this case, the structure of the monopole is as follows: a soliton in the  $m_F = 1$  component, a vortex line with unit circulation in the  $m_F = 0$  component, and a doubly quantized vortex line in the  $m_F = -1$  component, where the strength of SO coupling  $\kappa = 2$ , the spin-dependent interaction coefficient  $\lambda_2 = -15$ . For all the bounded density isosurfaces and the slice plane density, which are capped with a density color map, where the optical trap frequencies are given by  $\omega_r = \omega_z = 2\pi \times 250\text{Hz}$ , the magnetic field gradient strength  $B_1 = 0.6$ , the unit of the characteristic length of harmonic oscillator is  $\sqrt{\hbar/m\omega}$ , the unit of the magnetic field gradient strength is  $(g_F\mu_B a_h)/(\omega\hbar)$ , and the unit of SO coupling strength is  $\sqrt{\hbar\omega/m}$ , the scale for three dimension system is  $34.2\mu m \times 34.2\mu m \times 34.2\mu m$ , and the scale for slice planes is  $34.2\mu m \times 34.2\mu m$ .

**Figure 3 The effect of strong spin-orbit coupling on the monopoles.** The particle densities of monopoles with weak spin-orbit (SO) coupling according to  $x \leq 0$  and  $z \leq 0$  are displayed in **(a1)** and **(b1)**. The phase distributions of the slice planes with  $x = 0$  are shown in **(a2)**. The phase distributions of the slice planes with  $z = 0$  are shown in **(b2)**, the black arrows indicate phases directions of the slice plane with  $x = 0$ . For **(a1-b2)**, the strength of SO coupling  $\kappa = 2$ . The particle densities of monopoles with strong SO coupling according to  $x \leq 0$  and  $z \leq 0$  are plotted in **(c1)** and **(d1)**. The phase distributions of the slice planes with  $x = 0$  are shown in **(c2)**. The phase distributions of the slice planes with  $z = 0$  are shown in **(d2)**, the black arrows indicate phases directions of the slice plane with  $x = 0$ . For **(c1-d2)**, the strength of SO coupling  $\kappa = 16$ . For all the bounded density isosurfaces and the slice plane density, which are capped with a density color map, for all figures, the magnetic field gradient strength  $B_1 = 0.6$ , the optical trap frequencies are given by  $\omega_r = \omega_z = 2\pi \times 250\text{Hz}$ , the unit of the characteristic length of harmonic oscillator is  $\sqrt{\hbar/m\omega}$ , the unit of the magnetic field gradient strength is  $(g_F\mu_B a_h)/(\omega\hbar)$ , and the unit of SO coupling strength is  $\sqrt{\hbar\omega/m}$ , the scale for three dimension system is  $34.2\mu m \times 34.2\mu m \times 34.2\mu m$ , and the scale for slice planes is  $34.2\mu m \times 34.2\mu m$ .

**Figure 4 The effect of anisotropic spin-orbit coupling on the monopoles.** **(a-c)** Particle densities and phase distributions the corresponding the three spin components under the anisotropic spin-orbit (SO) coupling. The first column indicates the density isosurfaces of each component, from the second column to the third column display the densities and phase distributions of the slice plane of  $z = 0$  the corresponding each component, the black arrows indicate phases directions of the slice plane with  $z = 0$ . From the fourth column to the fifth column show the densities and

phase distributions of the slice plane of  $x = 0$  the corresponding each component, the colour map is given in the last row. For all figures, the strength of anisotropic SO coupling  $\kappa_x = 8$  and  $\kappa_y = 2$ , the optical trap frequencies are given by  $\omega_r = \omega_z = 2\pi \times 250\text{Hz}$ , the magnetic field gradient strength  $B_1 = 0.6$ , the unit of the characteristic length of harmonic oscillator is  $\sqrt{\hbar/m\omega}$ , the unit of the magnetic field gradient strength is  $(g_F\mu_B a_h)/(\omega\hbar)$ , and the unit of SO coupling strength is  $\sqrt{\hbar\omega/m}$ , the scale for three dimension system is  $34.2\mu m \times 34.2\mu m \times 34.2\mu m$ , and the scale for slice planes is  $34.2\mu m \times 34.2\mu m$ .

**Figure 5 Spin textures of the monopoles.** (a) The spin textures of the monopoles for weak spin-orbit (SO) coupling strength  $\kappa = 2$ . (b) The spin textures of the monopoles for strong SO coupling strength  $\kappa = 16$ . (c) The spin textures of the monopoles for anisotropic SO coupling  $\kappa_x = 8$  and  $\kappa_y = 2$ . For all figures, where the slice planes are  $z = 5$ ,  $y = 5$  and  $x = 5$ , the magnetic field gradient strength  $B_1 = 0.6$ , the optical trap frequencies are given by  $\omega_r = \omega_z = 2\pi \times 250\text{Hz}$ , the unit of the characteristic length of harmonic oscillator is  $\sqrt{\hbar/m\omega}$ , the unit of the magnetic field gradient strength is  $(g_F\mu_B a_h)/(\omega\hbar)$ , and the unit of SO coupling strength is  $\sqrt{\hbar\omega/m}$ , the scale for slice planes is  $34.2\mu m \times 34.2\mu m$ .

**Figure 6 The phase diagrams of the monopoles.** (a) The phase diagram of the monopole in spinor Bose-Einstein condensates depicted by spin-orbit (SO) coupling strength  $\kappa$  and spin-independent interaction parameter  $\lambda_0$ , where spin-dependent interaction parameter  $\lambda_2 = -75$ . (b) The phase diagram of the monopole in spinor Bose-Einstein condensates depicted by SO coupling strength  $\kappa$  and spin-dependent interaction constant  $\lambda_2$ , spin-independent interaction parameter is

given by  $\lambda_0 = 7500$ . All the phases in these two phase diagrams of monopoles, consist of the metastable (MS) phase, the polar-core vortex (PCV) phase, the Mermin-Ho vortex (MHV) phase, and the square lattice (SL) phase, where the magnetic field gradient strength  $B_1 = 0.6$ , the optical trap frequencies are given by  $\omega_r = \omega_z = 2\pi \times 250\text{Hz}$ , the unit of the characteristic length of harmonic oscillator is  $\sqrt{\hbar/m\omega}$ , the unit of the magnetic field gradient strength is  $(g_F\mu_B a_h)/(\omega\hbar)$ , and the unit of SO coupling strength is  $\sqrt{\hbar\omega/m}$ , the scale for three dimension system is  $34.2\mu m \times 34.2\mu m \times 34.2\mu m$ .

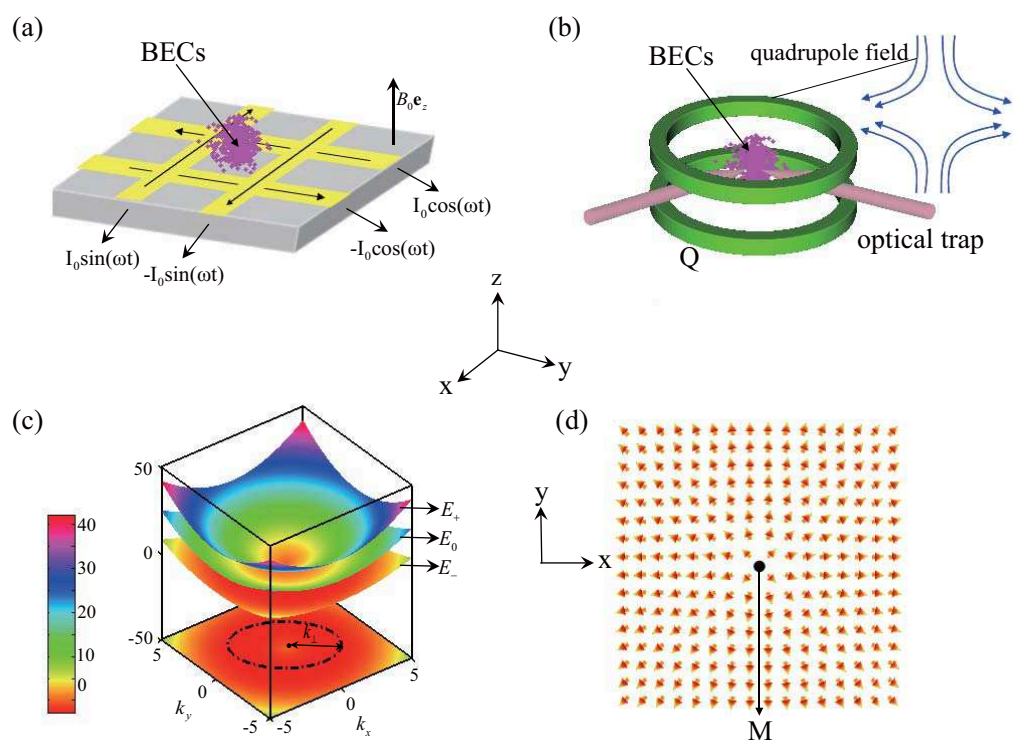


Figure 1



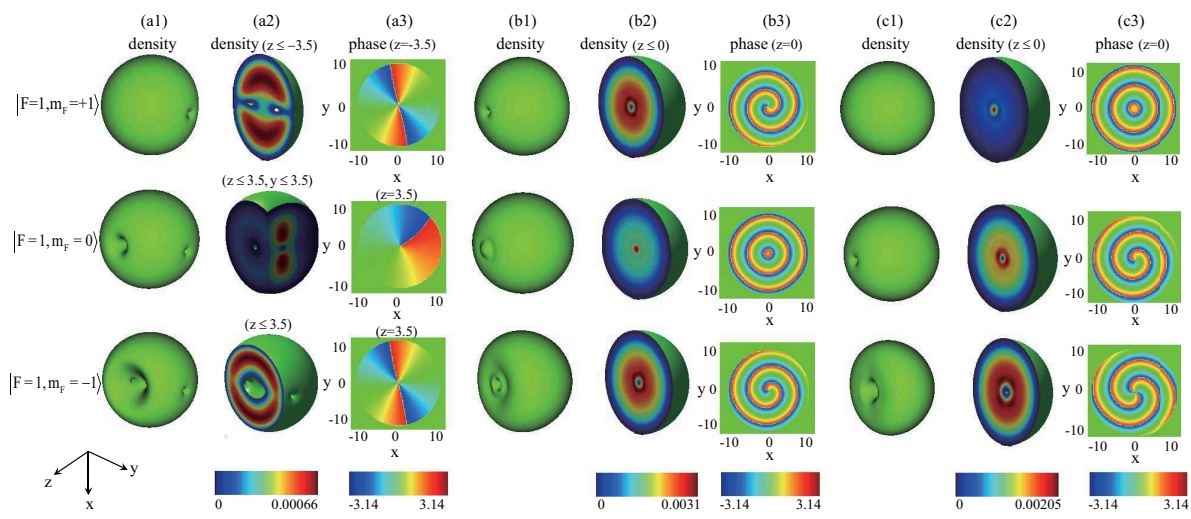


Figure 2

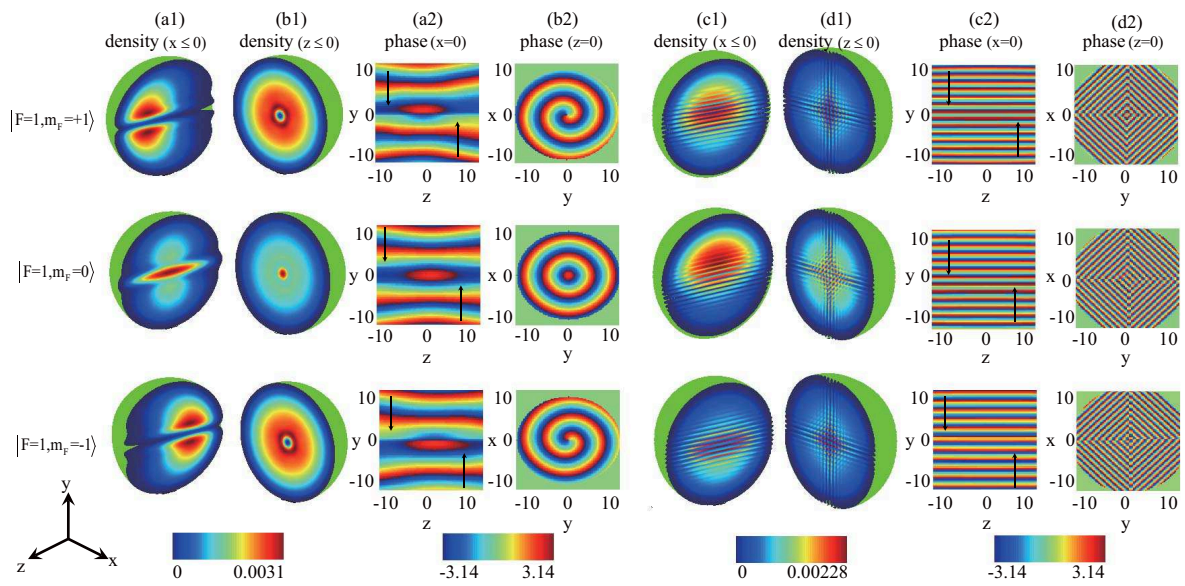


Figure 3

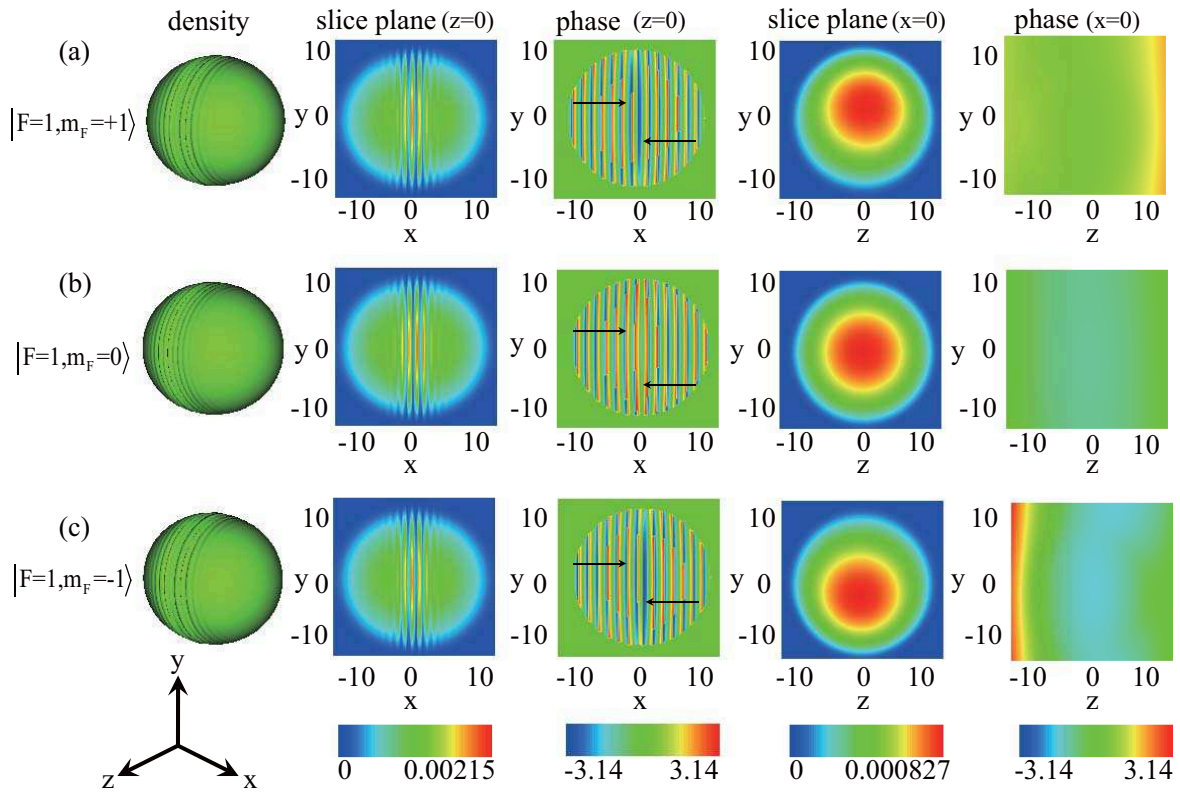


Figure 4

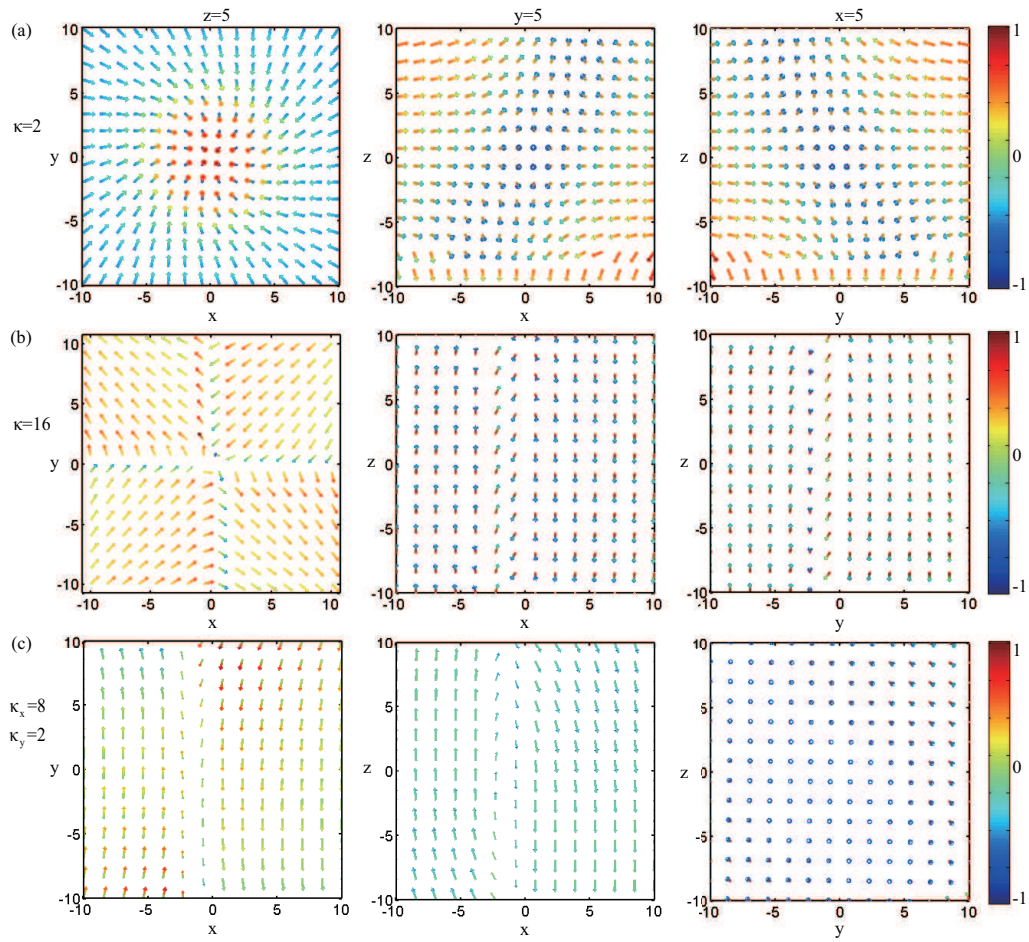


Figure 5

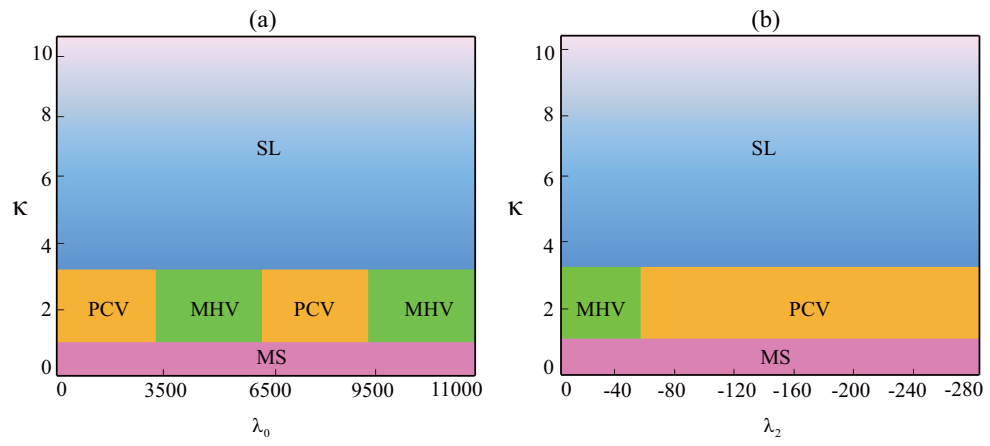


Figure 6